

1 **Cloud scavenging of anthropogenic refractory particles at a mountain site in**  
2 **North China**

3  
4 Lei Liu<sup>1,2</sup>, Jian Zhang<sup>2</sup>, Liang Xu<sup>1,2</sup>, Qi Yuan<sup>2</sup>, Dao Huang<sup>2</sup>, Jianmin Chen<sup>3</sup>, Zongbo Shi<sup>4</sup>, Yele Sun<sup>5</sup>,  
5 Pingqing Fu<sup>5</sup>, Zifa Wang<sup>5</sup>, Daizhou Zhang<sup>6</sup>, Weijun Li<sup>2,\*</sup>

6  
7 <sup>1</sup>Environment Research Institute, Shandong University, Jinan 250100, China

8 <sup>2</sup>Department of Atmospheric Sciences, School of Earth Sciences, Zhejiang University, Hangzhou 320007, China

9 <sup>3</sup>Shanghai Key Laboratory of Atmospheric Particle Pollution and Prevention, Department of Environmental Science  
10 and Engineering, Fudan University, Shanghai 200433, China

11 <sup>4</sup>School of Geography, Earth and Environmental Sciences, University of Birmingham, Birmingham B15 2TT, UK

12 <sup>5</sup>State Key Laboratory of Atmospheric Boundary Layer Physics and Atmospheric Chemistry, Institute of Atmospheric  
13 Physics, Chinese Academy of Sciences, Beijing 100029, China

14 <sup>6</sup>Faculty of Environmental and Symbiotic Sciences, Prefectural University of Kumamoto, Kumamoto 862-8502, Japan

15 \*Correspondence to: Weijun Li (liweijun@zju.edu.cn)

16 **Abstract.** Aerosol-cloud interactions remain a major source of uncertainty in climate forcing estimate.  
17 Few studies have been conducted to characterize the aerosol-cloud interactions in heavily polluted  
18 conditions worldwide. In this study, cloud residual and cloud interstitial particles were collected during  
19 cloud events under different pollution levels from 22 July to 1 August, 2014 at Mt. Tai (1532 m above  
20 sea level) located in the North China Plain. A transmission electron microscope was used to investigate  
21 morphology, size, and chemical composition of individual cloud residual and cloud interstitial particles,  
22 and to study mixing properties of different aerosol components in individual particles. Our results show  
23 that S-rich particles were predominant (78%) during clean periods ( $PM_{2.5} < 15 \mu\text{g m}^{-3}$ ), but a large  
24 amount of anthropogenic refractory particles (e.g., soot, fly ash, and metal) and their mixtures with  
25 S-rich particles (named as S-refractory) were observed during polluted periods. Cloud droplets collected  
26 during polluted periods were found to become an extremely complicated mixture by scavenging  
27 abundant refractory particles. We found that 76% of cloud residual particles were S-refractory particles  
28 and that 26% of cloud residual particles contained two or more types of refractory particles.  
29 Soot-containing particles (i.e., S-soot and S-fly ash/metal-soot) were the most abundant (62%) among  
30 cloud residual particles, followed by fly ash/metal-containing particles (i.e., S-fly ash/metal and S-fly  
31 ash/metal-soot, 37%). The complicated cloud droplets have not been reported in clean continental or  
32 marine air before. Our findings provide an insight into the potential impacts on cloud radiative forcing  
33 from black carbon and metal catalyzed reactions of  $SO_2$  in micro-cloud droplets containing soluble  
34 metals released from fly ash and metals over polluted air.

## 35 **1. Introduction**

36 Clouds play a crucial role in various physical and chemical processes occurring in the lower  
37 troposphere and hence affect the Earth's radiation budget (Seinfeld et al., 2016; Tilgner et al., 2014).  
38 Aerosol particles, including primary and secondary ones generated from natural and anthropogenic  
39 sources, either directly alter radiative forcing or act as cloud condensation nuclei (CCN) to indirectly  
40 influence it. At present, aerosol-cloud interactions unquestionably affect radiative forcing and global  
41 climate (McFiggans et al., 2006; Rosenfeld et al., 2014; Seinfeld and Pandis, 2006). CCN become cloud  
42 droplets through the condensation of water vapor when the relative humidity (RH) of an air parcel  
43 increases above saturation (Farmer et al., 2015). Size, chemical composition, and mixing state are main  
44 factors affecting the ability of a particle to act as CCN (Dusek et al., 2006; Fan et al., 2016; Hudson,  
45 2007; Li et al., 2011a; Rosenfeld, 2000). In addition, aerosol particles incorporated into cloud droplets  
46 can be easily lifted into the free troposphere during cloud development and further extend their  
47 influence on cloud precipitation and regional climate (Fan et al., 2016).

48 Owing to the rapid industrialization and urbanization in Asia, large quantities of aerosol particles  
49 from anthropogenic sources are released into the atmosphere, which can dramatically affect the  
50 chemical composition of CCN, and furthermore change the properties of clouds such as radiative  
51 forcing, lifetime, and precipitation patterns (Drewnick et al., 2007; Ervens, 2015; Li et al., 2011b;  
52 Twohy and Anderson, 2008). High concentrations of aerosol particles increase the number of cloud  
53 droplets and reduce their size, which further results in the reduction of precipitation efficiency and in  
54 extending the lifetime of clouds (Fan et al., 2016; Li et al., 2017a; McFiggans et al., 2006; Qian et al.,  
55 2009; Rosenfeld, 2000). Moreover, anthropogenic aerosol particles - especially fly ash, metal, and soot  
56 particles - are incorporated into cloud droplets, and be transported long distances to affect ecosystems,  
57 human health, and radiative forcing (Li et al., 2013; Rosenfeld et al., 2014). Especially the toxic and  
58 bioaccumulative metals can deposit into the ecosystem following fog or precipitation and further cause  
59 severe health problems to human beings (Liu et al., 2012). Moreover, transition metals such as iron (Fe)  
60 and manganese (Mn) can enhance the in-cloud oxidation of sulfur dioxide to sulfate (Harris et al.,  
61 2013).

62 Recently, many studies have been performed worldwide to investigate aerosol-cloud interactions  
63 and the composition of cloud droplets. Schroder et al. (2015) investigated the activation of refractory

64 black carbon particles in stratocumulus clouds at a marine boundary layer site using a counterflow  
65 virtual impactor and single particle soot photometer. Ueda et al. (2014) reported the effects of in-cloud  
66 processes on the compositional changes of sea salt particles by collecting individual aerosol particles in  
67 and below clouds, respectively. Pierce et al. (2015) calculated size distribution changes and radiative  
68 forcing effects due to the scavenging of interstitial particles by cloud droplets in a clean remote region.  
69 Roth et al. (2016) analyzed the composition and mixing state of cloud residues and out-of-cloud aerosol  
70 particles by single particle aerosol mass spectrometry on a mountain site and found that soot particles  
71 internally mixed with sulfate and nitrate were the dominant ones in cloud residues. All of the above  
72 studies were carried out in the clean atmosphere; they could not observe the clear interactions between  
73 abundant anthropogenic particles and cloud droplets. However, the latest satellite observations indicated  
74 that large amounts of anthropogenic fine particles assembled in cloud base and might modify cloud  
75 properties in heavily polluted air influenced by industrial and urban emissions (Eck et al., 2018). Field  
76 observations are needed to confirm it and understand the interactions of aerosol-cloud over polluted  
77 areas, especially in North and South Asia.

78 Mt. Tai, the highest mountain in the NCP, is surrounded by several medium-sized industrial cities.  
79 The altitude of Mt. Tai is close to the top of the planetary boundary layer (PBL) above the NCP.  
80 Therefore, Mt. Tai is an ideal site to study the effects of regional transport and local emissions of  
81 anthropogenic aerosols on cloud properties. Numerous studies have been conducted on Mt. Tai, but  
82 virtually all the researchers mainly focus on the variation of chemical composition and size distribution  
83 of aerosol particles (Zhang et al., 2014) and chemical composition of cloud water (Li et al., 2017a;  
84 Wang et al., 2011). Because of the limitation of sampling and analyzing techniques, these studies did  
85 not consider the aerosol-cloud interactions at the top of Mt. Tai in North China.

86 Transmission electron microscopy (TEM) has become a powerful technique to characterize the  
87 particle morphology, size, and composition and mixing properties of different components in individual  
88 particles in recent years (Li et al., 2016a; Ueda et al., 2014). Many studies used single particle aerosol  
89 mass spectrometry (SPAMS) to characterize the composition of residual particles of individual cloud  
90 droplets (Lin et al., 2017; Pratt et al., 2010; Zhang et al., 2017). Compared to the SPAMS, TEM can  
91 directly observe the morphology and different components of individual cloud droplet residual (cloud  
92 RES) and interstitial particles (cloud INT) (Kojima et al., 2004; Li et al., 2011a; Twohy and Anderson,  
93 2008; Ueda et al., 2014). Therefore, TEM technique can not only be used to identify cloud RES and

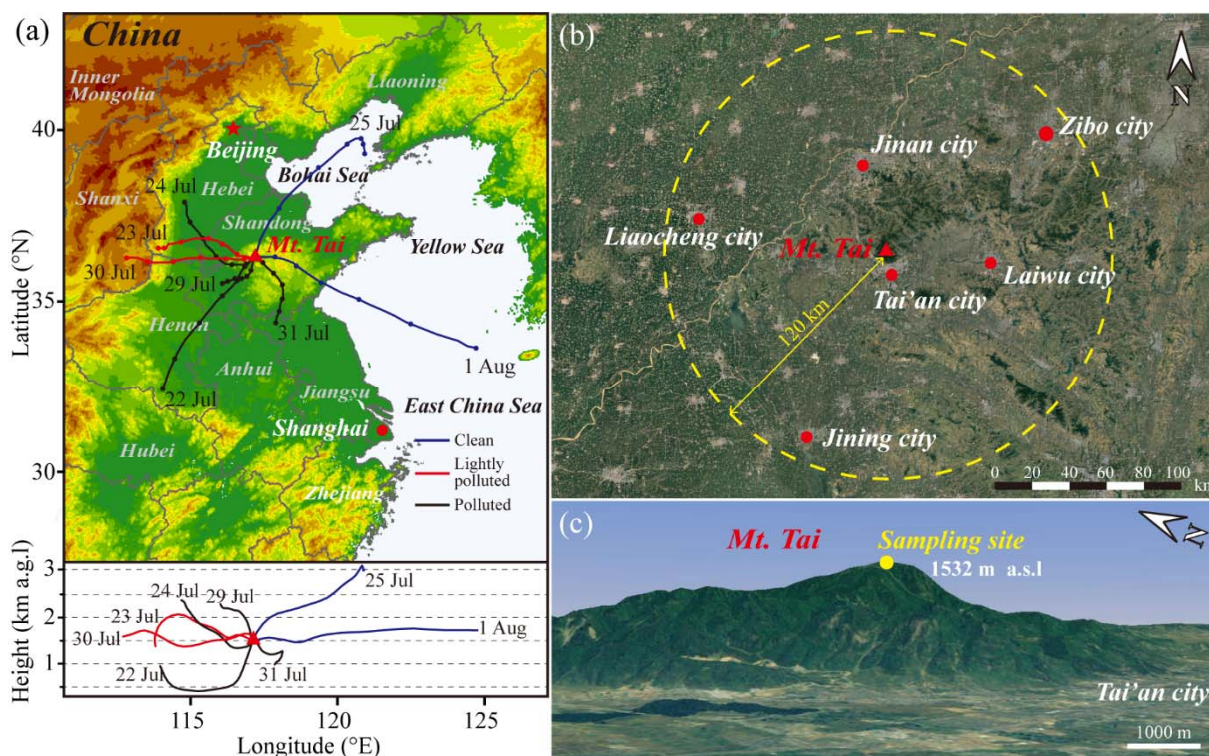
94 cloud INT collected in a same cloud event but also reveal interactions between aerosol-clouds based on  
95 the different components within individual particles. In this study, we collected individual particles  
96 during cloud events at the summit of Mt. Tai and applied TEM to obtain and compare the morphology,  
97 size, and composition of cloud RES and cloud INT. This is helpful to understand the influence of  
98 anthropogenic sources on cloud properties above the heavily polluted region.

## 99 **2. Experimental methods**

### 100 **2.1 Sampling sites**

101 Field observations were carried out at Mt. Tai (36.251°N, 117.101°E; 1532 m above sea level (a.s.l))  
102 from 22 July to 1 August 2014. Mt. Tai is the highest mountain in the central NCP and is surrounded by  
103 several medium-sized industrial cities (Fig. 1). A number of large coal-fired power plants, oil refinery  
104 plants, steel plants, and cement plants are located in these industrial cities (Jinan, Zibo, Laiwu,  
105 Liaocheng, Jining, Tai'an etc.) within a radius of 120 km around Mt. Tai (Fig. 1b). Jinan city is the  
106 capital of Shandong Province and is situated 60 km north of Mt. Tai. Tai'an city is located at the  
107 southern foot of Mt. Tai. Therefore, the local and regional emissions may have a large contribution to  
108 the air quality at the summit of Mt. Tai. Mt. Tai's altitude is close to the top of planetary boundary layer  
109 over the NCP, and local cloud events frequently occur at its summit, especially in summer.

110 As shown in Fig. 1c, individual particle samples were collected at a sampling site near the summit  
111 of Mt. Tai. The sampling site was usually covered by clouds when cloud events occurred during the  
112 sampling periods. The 24-h air mass backward trajectories arriving at Mt. Tai at 1500 m above ground  
113 level (a.g.l) (Fig. 1a) were calculated using the Hybrid Single-Particles Lagrangian Integrated Trajectory  
114 (HYSPLIT) model available at the NOAA Air Resources Laboratory's web server (Draxler and Rolph,  
115 2003).



116

117 **Figure 1.** (a) Location of Mt. Tai in the North China Plain and the 24-h air mass backward trajectories  
 118 arriving at Mt. Tai at 1500 m a.g.l during the sampling period. (b) The medium-sized industrial cities  
 119 distributed within a radius of 120 km around Mt. Tai. (c) The expanded topographic view of Mt. Tai and  
 120 the sampling site near the summit of Mt. Tai.

## 121 2.2 Individual particle collections

122 Individual aerosol particles were collected onto carbon films supported by TEM copper grids  
 123 (carbon type-B, 300-mesh copper, Beijing XXBR Technology Co., Ltd, China) using a single-stage  
 124 cascade impactor with a 0.5 mm diameter jet nozzle at a flow rate of 1.0 L min<sup>-1</sup>. The aerodynamic  
 125 diameter of particles collected with a 50% efficiency (cutoff diameter,  $d_{50}$ ) by the sampler is 0.24  $\mu\text{m}$  if  
 126 particle density is 2 g cm<sup>-3</sup>. More detailed information about the setup of a modified sampler can be  
 127 found in Li et al. (2011a). When cloud events occurred at the summit of Mt. Tai, individual particle  
 128 samples were collected during the cloud events except one cloud event in the late midnight of 26 July  
 129 (Fig. 3). The sample information in the present study is listed in Table 1.

130 During the sampling period, meteorological data at the summit of Mt. Tai including pressure (P),  
 131 relative humidity (RH), temperature (T), wind speed (WS), and wind direction (WD) were measured  
 132 and recorded every 5 min by a pocket weather meter (Kestrel 4500, Nielsen-Kellermann Inc., USA).  
 133 PM<sub>2.5</sub> concentrations on Mt. Tai were monitored on-line by a beta attenuation and optical analyzer

134 (model 5030 SHARP monitor, Thermo Scientific, USA).

135 **Table 1.** Information on individual particle samples collected on Mt. Tai.

Sample ID	Sampling time (local time)	PM <sub>2.5</sub> ( $\mu\text{g m}^{-3}$ )	T ( $^{\circ}\text{C}$ )	RH (%)	P (hPa)	WS ( $\text{m s}^{-1}$ )
1	22 Jul. 2014 16:04	51.6	22.8	100	849.1	0.9
2	23 Jul. 2014 08:00	24.2	20.4	100	849.4	2.5
3	24 Jul. 2014 07:43	74.3	19.2	100	848.0	0
4	25 Jul. 2014 17:00	11.8	13.9	100	838.0	5.5
5	29 Jul. 2014 16:18	72.9	20.8	95.7	848.0	1.1
6	30 Jul. 2014 19:24	24.2	17.5	100	844.2	0.8
7	31 Jul. 2014 17:30	56.4	18.1	100	849.0	0.9
8	01 Aug. 2014 17:56	14.7	18.8	100	849.1	1.8

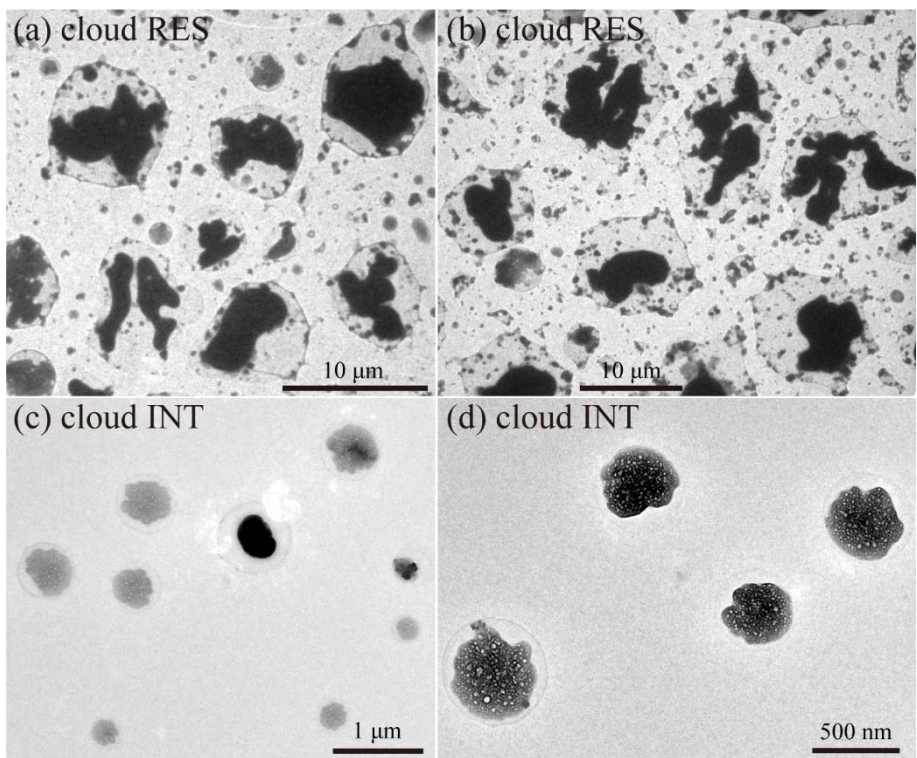
### 136 2.3 TEM analysis

137 Individual aerosol particles collected on TEM grids were analyzed by a transmission electron  
138 microscope (TEM, JEM-2100, JEOL Ltd., Japan) at a 200 kV accelerating voltage. TEM is equipped  
139 with an energy-dispersive X-ray spectrometer (EDS, INCA X-Max<sup>N</sup> 80T, Oxford Instruments, UK).  
140 EDS semi-quantitatively detects the elemental composition of individual particles with atomic number  
141 greater than six ( $Z > 6$ ). However, Cu peaks in the EDS spectra were not considered because of the  
142 interference from the copper substrate of TEM grids. We acquired morphology and composition of  
143 individual particles through the combination of TEM and EDS (TEM/EDS).

144 The distribution of aerosol particles on TEM grids was not uniform, with particle size decreasing  
145 from the center to the edge of the TEM grids. Cloud droplets with larger size normally impacted on the  
146 center and interstitial particles mostly distributed on the peripheral areas of TEM grids (Li et al., 2011a).  
147 Moreover, cloud RES had large rims compared with cloud INT, suggesting that cloud RES were  
148 droplets before being captured (Zhang et al., 2006). According to the distribution and morphology of  
149 individual particles on the substrate, we can distinguish between cloud RES and cloud INT particles.  
150 Figure 2 generally displays typical TEM images of cloud RES and cloud INT particles. Generally, a  
151 number of previous studies using the cascade impactor have successfully captured individual interstitial  
152 particles and cloud droplets on the substrate during cloud events (Kojima et al., 2004; Li et al., 2011a;

153 Ueda et al., 2014; Zhang et al., 2006).

154 To obtain the size of cloud RES and cloud INT particles, we measured the area and equivalent  
155 circle diameter (ECD) of these analyzed particles by iTEM software (Olympus soft imaging solutions  
156 GmbH, Germany). It should be noted that we measured ECD of the core of individual cloud RES  
157 excluding the water rim because water rim only contains trace organics (Li et al., 2011a). The ECD can  
158 be further converted to equivalent spherical diameter (ESD) according to the AFM analysis (refer to the  
159 Supplement Fig. S1).



160

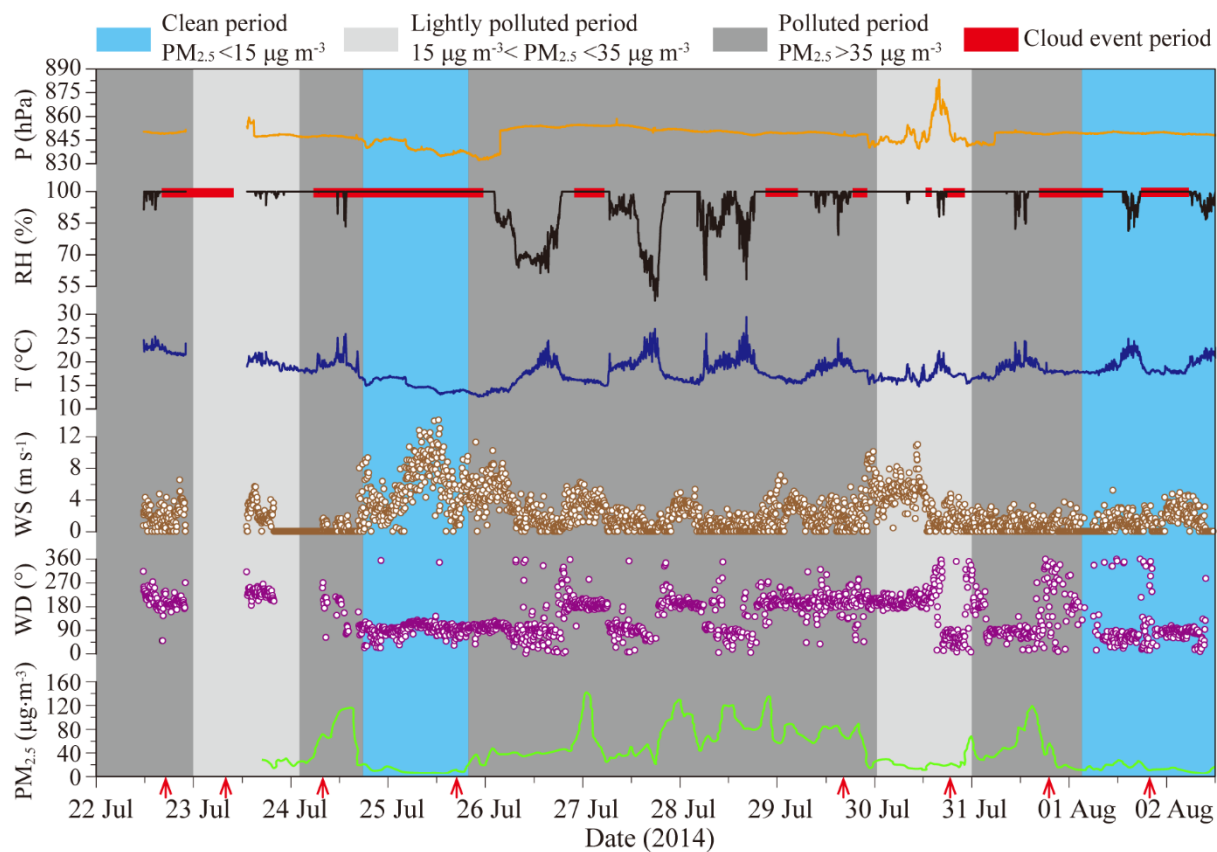
161 **Figure 2.** Low magnification TEM images of cloud RES (a-b) and cloud INT (c-d) particles collected  
162 on Mt. Tai.



## 163 **3. Results**

### 164 **3.1 Meteorological conditions and backward trajectories**

165 Temporal variations of pressure (P), relative humidity (RH), temperature (T), wind speed (WS),  
166 wind direction (WD), and PM<sub>2.5</sub> concentration were measured on Mt. Tai from 22 July to 2 August 2014  
167 (Fig. 3). During the sampling period, the temperature ranged from 12.6 to 29.4 °C, and the RH varied  
168 between 48.2% and 100%. Each day during the sampling period, the RH reached 100% as temperatures  
169 decreased from the late afternoon into the evening (Fig. 3). We noticed that PM<sub>2.5</sub> concentrations on the  
170 mountaintop were closely related to wind direction and speed during the regional transport of hazes.  
171 Based on backward trajectories of air masses and PM<sub>2.5</sub> concentrations, the whole sampling period can  
172 be divided into three categories: *clean period* (PM<sub>2.5</sub> < 15 μg m<sup>-3</sup>), the prevailing winds were from the  
173 northeast to east and air masses were from higher altitudes above the marine areas which lead to the  
174 lowest PM<sub>2.5</sub> concentration; *lightly polluted period* (15 μg m<sup>-3</sup> < PM<sub>2.5</sub> < 35 μg m<sup>-3</sup>), the prevailing  
175 winds were from the west, and air masses originating from higher altitudes above continental areas  
176 brought regional pollutants to the summit of Mt. Tai; *polluted period* (PM<sub>2.5</sub> > 35 μg m<sup>-3</sup>), air masses  
177 originating from northwest, southwest, or south went through Tai'an city. Back trajectories as shown in  
178 Fig. 1a during polluted days suggest that air pollutants from industrialized cities might be lifted along  
179 the southern slope up to Mt. Tai's summit.



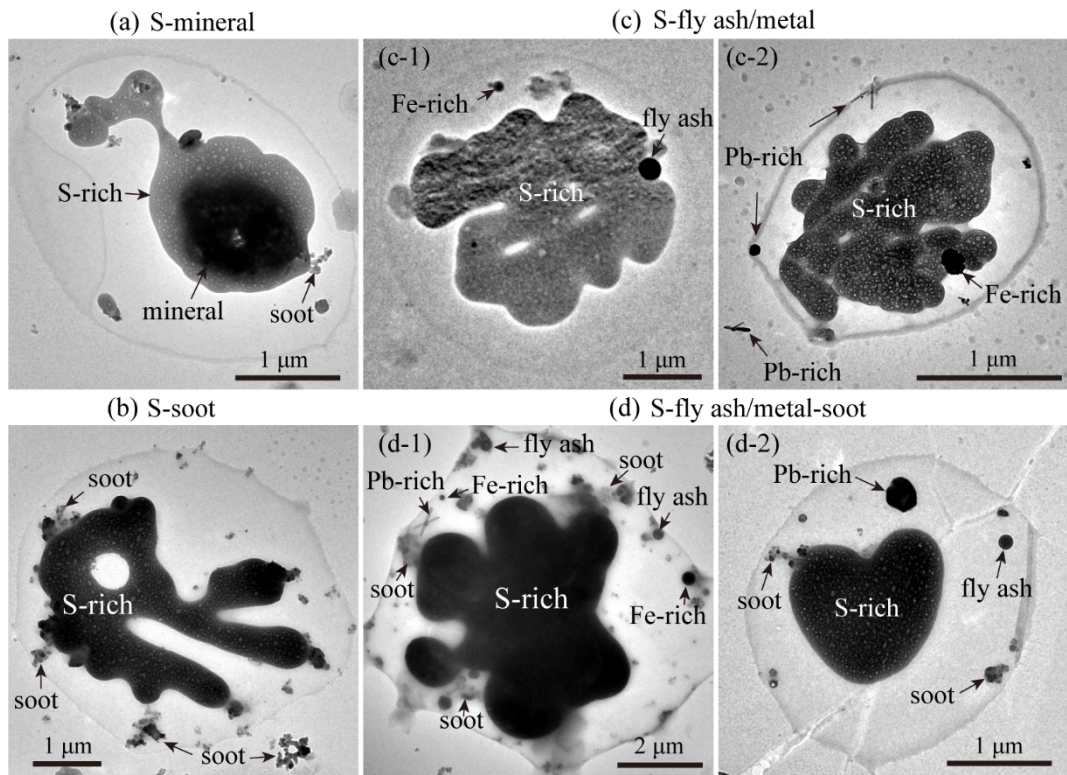
180

181 **Figure 3.** Temporal variations of pressure (P), relative humidity (RH), temperature (T), wind speed  
 182 (WS), and wind direction (WD) measured on Mt. Tai from 22 July to 2 August 2014. The red arrows  
 183 indicate collection times of individual particle samples during the cloud events.

### 184 **3.2 Mixing properties of anthropogenic refractory particles**

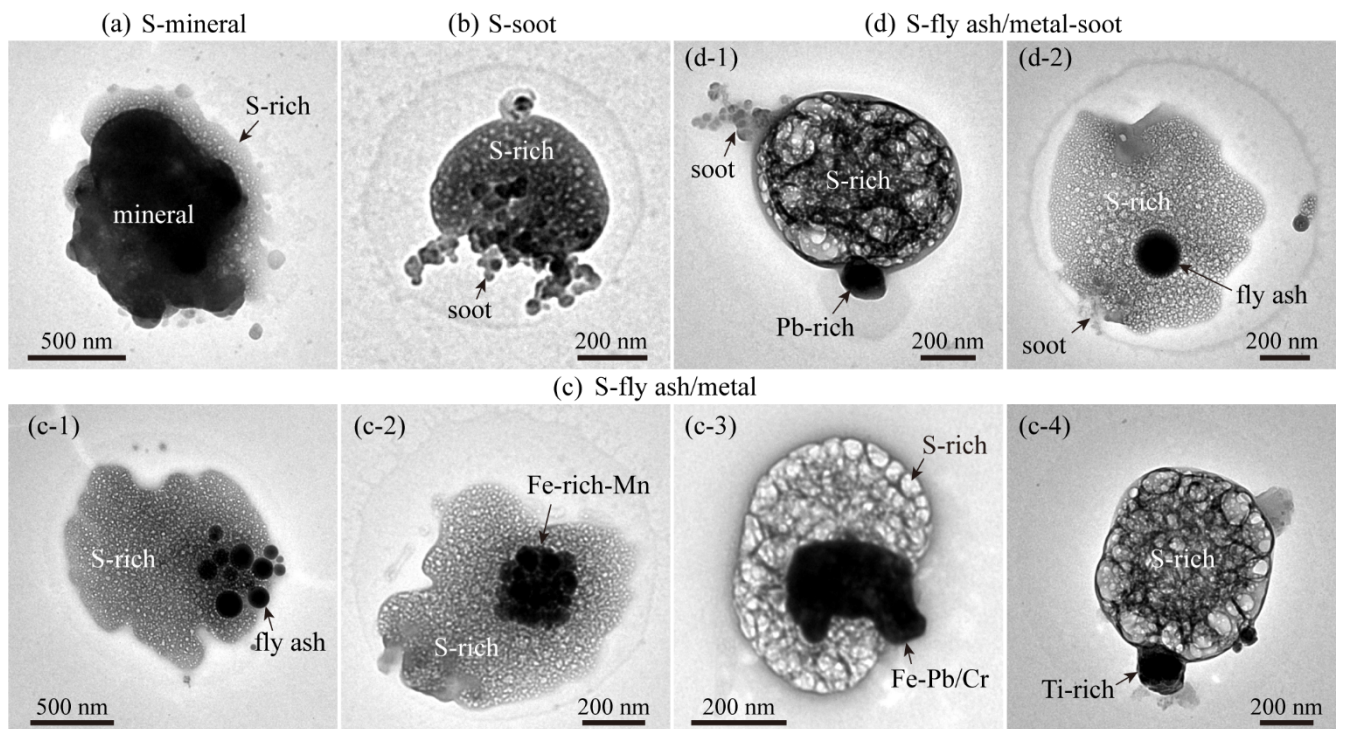
185 Based on the elemental composition and morphology of individual particles, six basic types of  
186 individual particles were classified: S-rich (Fig. S2a), soot (Fig. S2b), organic matter (OM, Fig. S2c),  
187 mineral (Fig. S2d), and fly ash/metal (Figs. S2e-h). The classification criteria of different particle types  
188 and their sources have been described in a separate study (Li et al., 2016a). S-rich particles representing  
189 secondary inorganic particles (e.g.,  $\text{SO}_4^{2-}$ ,  $\text{NO}_3^-$ , and  $\text{NH}_4^+$ ) are transformed from gaseous  $\text{SO}_2$ ,  $\text{NO}_x$ ,  
190 and  $\text{NH}_3$ . OM can be divided into primary organic matter (POM) and secondary organic matter (SOM).  
191 POM is directly emitted from coal or biomass burning and normally has spherical or irregular shapes  
192 (Liu et al., 2017), whereas SOM is produced from the chemical oxidation of volatile organic compounds  
193 (VOCs) and exhibits OM-coating on S-rich particles (Li et al., 2016b). Fly ash (e.g., Si, Al, and O) and  
194 metal particles (e.g., Fe, Mn, Zn, and Pb) normally are emitted from coal-fired power plants and heavy  
195 industrial activities, such as production activities in steel mills and smelters. Soot particles are generated  
196 from incomplete combustion processes of biomass burning and fossil fuels in both industrial activities  
197 and vehicular emissions. In much of the climate-change and environmental literature, “soot” and “black  
198 carbon” are commonly used interchangeably, and “black carbon” is the most commonly used term in  
199 the climate-science community (Andreae and Gelencsér, 2006; Buseck et al., 2014). In the following  
200 sections, we use the term “soot” for the classification of particle types and the term “black carbon” for  
201 the discussion of the climate issues. Mineral particles come from construction activities, resuspended  
202 road dust, and natural soil. Among these types of particles, soot, POM, fly ash, mineral, and metal  
203 particles were refractory under electron beams and were thus termed as refractory particles (Ebert et al.,  
204 2016).

205 Based on mixing properties of multi-components within individual particles (Figs. 4 and 5), these  
206 particles can be further classified into four categories: S-mineral (Figs. 4a and 5a), S-soot (Figs. 4b and  
207 5b), S-fly ash/metal (Figs. 4c and 5c), S-fly ash/metal-soot (Figs. 4d and 5d). Here, these four types of  
208 particles with refractory inclusions are generally defined as “S-refractory” particles.



209

210 **Figure 4.** Typical TEM images showing mixing properties of multi-components within individual cloud  
 211 RES particles: (a) a mixture of S-rich and mineral; (b) a mixture of S-rich and soot; (c) a mixture of  
 212 S-rich and fly ash/metal; (d) a mixture of S-rich, soot, and fly ash/metal.



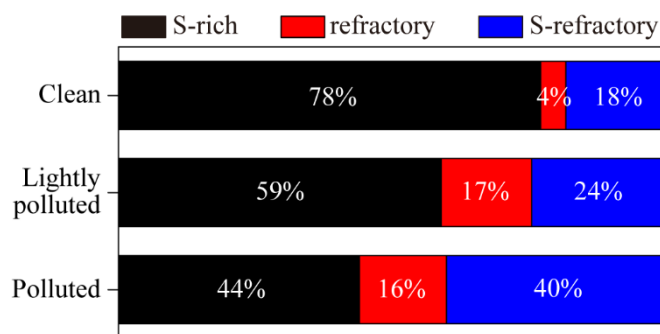
213

214 **Figure 5.** Typical TEM images showing mixing properties of multi-components within individual cloud  
 215 INT particles: (a) a mixture of S-rich and mineral; (b) a mixture of S-rich and soot; (c) a mixture of  
 216 S-rich and fly ash/metal; (d) a mixture of S-rich, soot and fly ash/metal.

217

218 Figure 6 shows number fractions of S-rich, refractory, and S-refractory particles in clean, lightly  
219 polluted, and polluted periods on Mt. Tai. In clean periods, S-rich particles had the highest proportion  
220 (78%), followed by a 22% contribution of the refractory and S-refractory particles. This may be  
221 attributed to the clean air masses that originated from the clean marine area and arrived at the summit of  
222 Mt. Tai through high-altitude transport (above 1500 m) (Fig. 1). Because the air masses did not contact  
223 the ground surface, the local anthropogenic pollutants (e.g., soot, fly ash, and metal) could not be lifted  
224 to the summit of Mt. Tai. Hence, secondary particles like S-rich were dominant in the clean period. In  
225 the lightly polluted and polluted periods, the fraction of S-rich particles decreased to 59% and 44%,  
226 respectively; meanwhile, the fractions of refractory and S-refractory increased up to 41% and 56%,  
227 respectively (Fig. 6). The backward trajectories suggest that these air masses went through the most  
228 heavily polluted areas before they arrived at the mountaintop (Fig. 1). Air masses on two polluted days  
229 (e.g., 22 and 31 July) were lifted from ground level to the atmospheric boundary layer. Our study shows  
230 that number fractions of refractory and S-refractory particles significantly increased from clean to  
231 polluted periods (Fig. 6). This result shows that large amounts of primary refractory particles from  
232 ground-level anthropogenic sources were lifted into the upper air and were further internally mixed with  
233 S-rich particles.

234



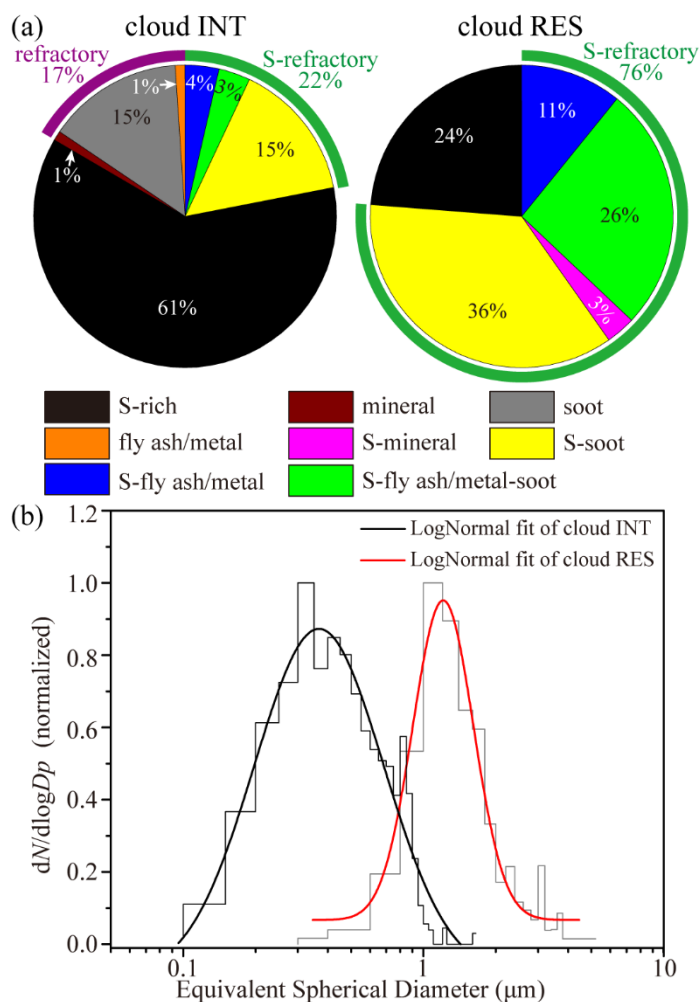
235 **Figure 6.** Number fractions of S-rich, refractory, and S-refractory particles at different pollution levels.

### 236 3.3 Comparisons of cloud RES and INT particles

237 During the sampling period, a fog monitor was used to measure the size of cloud droplets during  
238 cloud events (Li et al., 2017a). This study reveals that in the cloud events all the cloud droplets  
239 displayed particle size larger than 2  $\mu\text{m}$  in which size range the interstitial particles were absent. Based  
240 on their different size, we can know that these cloud droplets and interstitial particles impacted on  
241 different positions on the substrate. Although cloud droplets and interstitial particles became dry after  
242 the collection, they can still be identified based on the distribution and morphology of individual  
243 particles in TEM images (Kojima et al., 2004; Li et al., 2011a; Ueda et al., 2014; Zhang et al., 2006).  
244 Cloud RES display larger size and large rims around their CCN (Figs. 2 and 4) which has not been  
245 observed in non-cloud events. In contrast, cloud INT impacted on the position away from the center of  
246 sampling spot and their morphology looks like individual particles collected in non-cloud events.  
247 According to the rule, we can identify cloud RES and cloud INT in the samples collected during the  
248 cloud events.

249 Figure 7a shows that 100% of cloud RES and 83% of cloud INT contained S-rich species (i.e.,  
250 S-rich and S-refractory). In other words, none of cloud RES were soot, fly ash/metal, and mineral  
251 particles but 17% of cloud INT were. Soot particles mainly distributed in the finer size bins ( $< 600$  nm)  
252 of cloud INT (Fig. S3a). Interestingly, we found that 76% of cloud RES were a mixture of sulfates and  
253 refractory particles, which is 3.5 times of 22% in cloud INT (Fig. 7a). Furthermore, 26% of cloud RES  
254 had two or more types of inclusions (i.e., S-fly ash/metal-soot in Figs. 4d and 5d) but only 3% of cloud  
255 INT did. Therefore, we can conclude that cloud RES are extremely complex mixtures formed when  
256 cloud droplets act like a collector to scavenge these refractory particles.

257 The size-resolved number fractions of different particle types in cloud RES and cloud INT indicate  
258 that S-rich particles were predominant from 60 nm to 1.2  $\mu\text{m}$  in cloud INT (Fig. S3a), and S-refractory  
259 particles (indicated by the red box) dominated from 400 nm to 5.5  $\mu\text{m}$  in cloud RES (Fig. S3b). Figure  
260 7b shows that the median diameters of cloud RES and cloud INT were 1.19  $\mu\text{m}$  and 422 nm,  
261 respectively. The size of cloud RES was much larger than that of cloud INT, suggesting that size is an  
262 important factor affecting the CCN ability (Dusek et al., 2006).



263  
 264 **Figure 7.** Number fractions of different particle types in cloud RES and INT particles (a) and size  
 265 distributions of cloud RES and cloud INT particles (b). The measured particle sizes exclude the effects  
 266 of water rims in TEM images. In total, 292 cloud RES and 1161 cloud INT particles were analyzed.

267 **4. Discussion**

268 TEM observations in this study reveal that cloud RES contained large amounts of  
 269 refractory-containing particles primarily emitted from various anthropogenic sources in the heavily  
 270 polluted NCP. As much as 76% of cloud RES were identified as S-refractory particles (Fig. 7a). We  
 271 found that soot-containing particles (i.e., S-soot and S-fly ash/metal-soot) were the most abundant (62%)  
 272 among the cloud RES, followed by the relatively abundant fly ash/metal-containing particles (i.e., S-fly  
 273 ash/metal and S-fly ash/metal-soot, 37%) compared with 18% and 7% in the cloud INT, respectively  
 274 (Fig. 7a). Although these refractory particles such as soot with hydrophobic properties could not be  
 275 CCN directly, they can be easily accumulated by the existing cloud droplets as inclusions (Zuberi et al.,  
 276 2005). In the heavily polluted NCP, large amounts of soot and fly ash/metal particles are released from  
 277 anthropogenic sources (e.g., industrial activities and vehicular exhaust). During cloud events, abundant



278 refractory particles can be efficiently entrained into existing liquid cloud droplets by wet scavenging. Li  
279 et al. (2011a) reported that particle number decreased dramatically during cloud formation at Mt. Tai  
280 with a scavenging ratio of 0.54, which demonstrated that aerosol particles could efficiently be  
281 incorporated into cloud droplets. Physical coagulation of interstitial particles with cloud droplets is an  
282 important process in developing clouds, which can lead to the reduction of cloud INT number and a size  
283 increase of cloud RES after the clouds dry (Pierce et al., 2015). As we know so far, the extremely  
284 complicated mixture of secondary and primary particles observed in the present study has seldom been  
285 found in cloud droplets in clean air over developed countries (Hao et al., 2013; Kojima et al., 2004;  
286 Schneider et al., 2017; Ueda et al., 2014), remote areas (Hiranuma et al., 2013), and ocean (Hopkins et  
287 al., 2008; Twohy and Anderson, 2008; Zhang et al., 2006). For example, Zhang et al. (2006) reported  
288 that S-rich particles were predominant in the cloud RES with a small number fraction of sea salt  
289 particles over the Sea of Japan and soot or fly ash/metal particles were not observed. The present study  
290 reveals that individual cloud droplets are a far more complicated system in polluted air in North China  
291 than in the pristine continental and clean ocean air of the world.

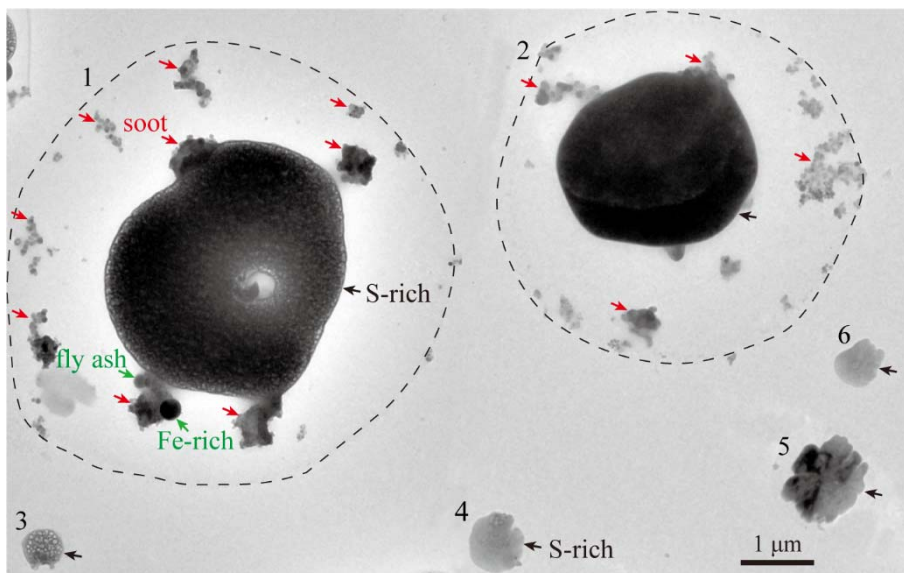
292 The cloud properties such as albedo and lifetimes could be largely modified by the aerosol-cloud  
293 interactions, especially in heavily polluted regions (Wang et al., 2010; Wang et al., 2013). The model  
294 simulation revealed that black carbon aerosols had a noticeable impact (up to nearly 20%) on cloud  
295 droplet number concentration in polluted black carbon source regions (Cherian et al., 2017). Especially,  
296 abundant black carbon particles incorporated into cloud droplets could lead to a decrease in cloud  
297 albedo by absorbing radiation and an increase of temperature in troposphere, then accelerate the  
298 evaporation of the cloud droplets (Ackerman et al., 2000; Adachi et al., 2010; Wang et al., 2013; Zuberi  
299 et al., 2005). In the past few decades, precipitation was significantly reduced over east-central China  
300 due to the large amounts of anthropogenic aerosols (Qian et al., 2009; Zhao et al., 2006). Because an  
301 excess of aerosols in clouds could reduce precipitation, the non-precipitating clouds in the NCP tend to  
302 evaporate back to aerosol particles by solar radiation. It is highly probable that abundant black carbon  
303 particles presenting in the cloud droplets in the heavily polluted NCP in this study (e.g., particle 1 and 2  
304 in Fig. 8) significantly affected the cloud properties and regional climate.

305 Fly ash and metal particles are a typical “fingerprint” pointing to the coal-fired power plants and  
306 boilers in factories and heavy industries (e.g., steel plant and smelting factory) (Chen et al., 2012; Li et  
307 al., 2016a; Moffet et al., 2008). Indeed, the most intense emissions from various industries in the world



308 occur in Hebei and Shandong provinces in the NCP (Qi et al., 2017). It is well known that these  
309 industrial activities continuously release anthropogenic pollutants via high stacks into the upper air. Liu  
310 et al. (2012) reported that the concentration of Zn reached  $249.1 \mu\text{g L}^{-1}$  in the cloud/fog water samples  
311 at Mt. Tai, followed by Al ( $157.3 \mu\text{g L}^{-1}$ ), Fe ( $105.8 \mu\text{g L}^{-1}$ ), Pb ( $46.2 \mu\text{g L}^{-1}$ ), and Mn ( $42.8 \mu\text{g L}^{-1}$ ),  
312 which were extremely higher than those values reported at Mt. Schmücke in Germany (Fomba et al.,  
313 2015). Combining these results with our present study, we infer that fine primary particles emitted from  
314 these industrial activities might spread and be lifted to the upper air more easily than at ground level.  
315 These metal particles, especially Pb and Zn of nanometer size, can harm ecosystems and human health  
316 (Roberts et al., 2004). The fly ash and metal particles incorporated into cloud droplets (e.g., particle 1 in  
317 Fig. 8) could go through the atmospheric acid Fe dissolution processes during long-range transport  
318 reported by Li et al. (2017b). If they were further transported to remote oceanic regions, soluble Fe  
319 species in the aerosol particles can fertilize plankton on the surface of ocean (Ito and Shi, 2016; Li et al.,  
320 2017b). Therefore, these anthropogenic fly ash/metal particles in polluted air contaminate cloud droplets  
321 and further amplify potential impacts of fine metal particles on the biogeochemical cycle in the  
322 troposphere.

323 Some studies suggested that the aqueous oxidation of  $\text{SO}_2$  to sulfate by  $\text{H}_2\text{O}_2$  and  $\text{O}_3$  in cloud  
324 droplets was dominant at Mt. Tai (Shen et al., 2012). However, cloud water collected on Mt. Tai  
325 contained high concentrations of soluble Fe, Mn, Zn, and Pb (Liu et al., 2012). These soluble metals in  
326 cloud droplets are released from aqueous reactions between metal particles and acidic sulfates in cloud  
327 droplets (Li et al., 2017b). Harris et al. (2013) estimated that the oxidation of  $\text{SO}_2$  in cloud droplets  
328 catalyzed by natural transition metal ions (TMIs) in mineral dust was dominant at Mt. Schmücke in  
329 Germany. For this study, how the soluble anthropogenic TMIs drive sulfate formation through TMI  
330 catalysis in micro-cloud droplets is still unresolved in polluted air. We propose that anthropogenic TMI  
331 catalysis contributing to sulfate production should be further studied in cloud droplets in the polluted  
332 NCP.



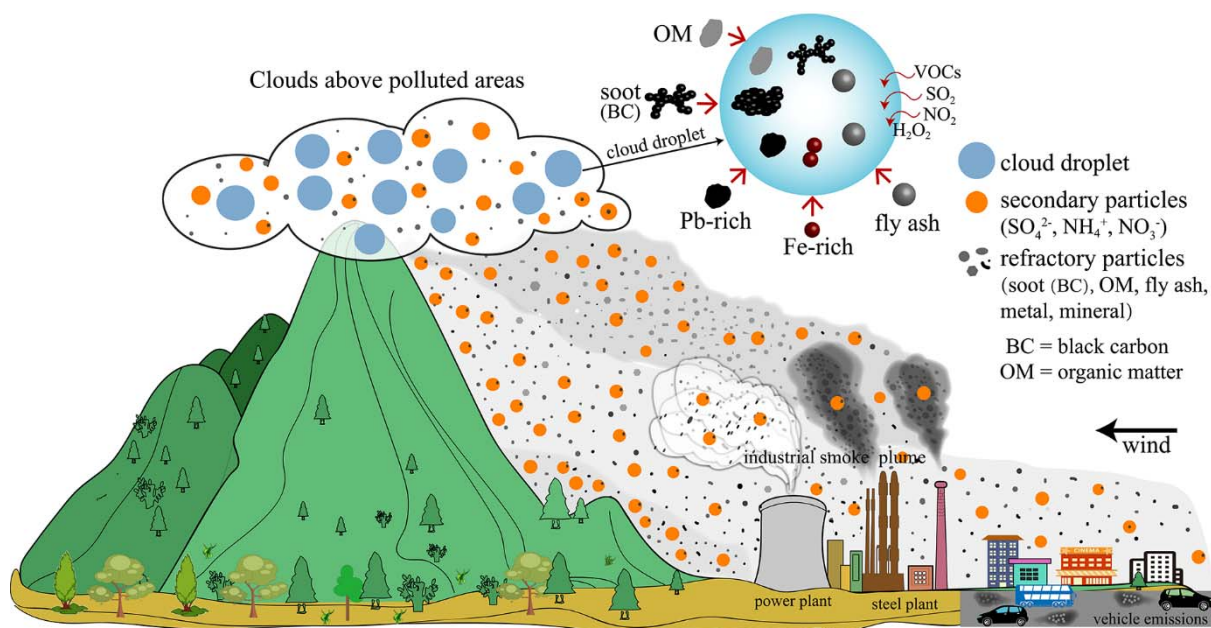
333

334 **Figure 8.** TEM image of cloud RES and INT particles collected during the cloud event occurred on the  
 335 polluted day of 31 July. Particle 1 and 2 are cloud RES and particle 3, 4, 5, and 6 are cloud INT. The  
 336 dashed lines indicate the water rims that were left after the cloud droplets impacting on the substrate  
 337 become dry.

338

339 The non-precipitating cloud processes over the polluted air of NCP quickly change the composition  
 340 of aerosol particles and cloud droplets in the upper air, potentially causing various effects such as  
 341 human health, regional climate, and biogeochemical cycle at the larger regional scale. To better  
 342 illustrate the aerosol-cloud interactions in this study, we created the conceptual model of Fig. 9. The tall  
 343 stacks of plants can emit smoke plumes that contain fine refractory particles and gaseous pollutants to  
 344 the upper air. A portion of particles in urban areas can also be lifted to the mountaintop by prevailing  
 345 valley winds. Once the clouds form on a mountaintop (or later are transported in other directions), these  
 346 cloud droplets act as collectors to scavenge the refractory particles. These refractory particles as  
 347 inclusions might complicate the cloud chemistry in micro-cloud droplets. Gaseous pollutants such as  
 348 SO<sub>2</sub>, NO<sub>x</sub>, and VOCs may have enhanced aqueous oxidation potential in the complex cloud droplets.  
 349 Our study is designed to better understand the aerosol-cloud interactions on the mountaintop in polluted  
 350 industrial and urban areas. Recently, a study showed that the major aerosol pollution events with very  
 351 high fine mode AOD (>1.0 in mid-visible) in the China-Korea-Japan region are often observed to be  
 352 associated with significant cloud cover (Eck et al., 2018). Therefore, we expect that large amounts of  
 353 fine refractory particles from polluted areas scavenging in clouds have important impacts not only at

354 local but also in large regional scale.



356 **Figure 9.** A conceptual model illustrating mechanisms of aerosol-cloud interactions on mountaintop  
357 influenced by anthropogenic pollutants from heavy industrial and urban emissions.

## 358 5. Conclusions

359 Individual aerosol particles were collected during cloud events on Mt. Tai from 22 July to 1 August,  
360 2014. Cloud RES and INT particles were separated by their distribution on TEM grids and their  
361 composition was identified by TEM/EDS. Individual particles were classified into S-rich, refractory (i.e.,  
362 mineral, soot, fly ash/metal) and S-refractory (i.e., S-mineral, S-soot, S-fly ash/metal, and S-fly  
363 ash/metal-soot). According to air mass backward trajectories and  $PM_{2.5}$  concentrations on Mt. Tai, the  
364 entire sampling period was divided into three classes: a clean period ( $PM_{2.5} < 15 \mu g m^{-3}$ ), a lightly  
365 polluted period ( $15 \mu g m^{-3} < PM_{2.5} < 35 \mu g m^{-3}$ ), and a polluted period ( $PM_{2.5} > 35 \mu g m^{-3}$ ). In the  
366 clean period, individual particles were dominated by S-rich particles (78%), whereas the fraction of  
367 refractory particles and S-refractory particles increased significantly and dominated during the polluted  
368 periods. This suggested that anthropogenic pollutants from tall stacks of coal-fired power plants and  
369 heavy industries and vehicular exhaust in cities could be lifted to the summit of Mt. Tai under the  
370 prevailing southerly winds in summer.

371 TEM observations showed that 76% of cloud RES were S-refractory particles contaminated by  
372 anthropogenic refractory particles, compared with only 22% of cloud INT. Cloud RES displayed a  
373 larger size than cloud INT, which indicates that particle size decidedly affects CCN ability. Our study

374 reveals that large amounts of anthropogenic refractory particles were incorporated into cloud droplets  
375 through in-cloud processes. Especially important is that abundant black carbon particles in cloud  
376 droplets could alter radiative forcing of clouds and accelerate the evaporation of cloud droplets. The  
377 high concentrations of transition metal ions might favor the aqueous-phase oxidation of SO<sub>2</sub> by O<sub>2</sub> in  
378 cloud droplets under the heavily polluted conditions in the NCP. Fly ash/metal-containing cloud  
379 droplets could be transported long distance and harm ecosystems and human health through wet  
380 deposition. We propose a conceptual model to show the aerosol-cloud interactions on mountaintops  
381 influenced by heavily polluted air.

382

383 **Data availability.** All data presented in this paper are available upon request. Please contact the  
384 corresponding author (liweijun\_atmos@gmail.com).

385

386 **Competing interests.** The authors declare that they have no conflict of interest.

387

388 **Acknowledgements.** We appreciate Peter Hyde's comments and proofreading. We thank Liang Wen at  
389 Shandong University for his assistance of sample collections. This work was funded by National Key  
390 R&D Program of China (2017YFC0212700), the National Natural Science Foundation of China  
391 (41575116, 41622504, and 41805099), State Key Laboratory of Atmospheric Boundary Physics and  
392 Atmospheric Chemistry (LAPC-KF-2017-02) and the Hundred Talents Program in Zhejiang University.

393 **References**

- 394 Ackerman, A. S., Toon, O. B., Stevens, D. E., Heymsfield, A. J., Ramanathan, V., and Welton, E. J.:  
395 Reduction of tropical cloudiness by soot, *Science*, 288, 1042-1047, 10.1126/science.288.5468.1042,  
396 2000.
- 397 Adachi, K., Chung, S. H., and Buseck, P. R.: Shapes of soot aerosol particles and implications for their  
398 effects on climate, *J. Geophys. Res.-Atmos.*, 115, D15206, 10.1029/2009JD012868, 2010.
- 399 Andreae, M. O., and Gelencsér, A.: Black carbon or brown carbon? The nature of light-absorbing  
400 carbonaceous aerosols, *Atmos. Chem. Phys.*, 6, 3131-3148, 10.5194/acp-6-3131-2006, 2006.
- 401 Buseck, P. R., Adachi, K., Gelencsér, A., Tompa, É., and Pósfai, M.: Ns-Soot: A Material-Based Term  
402 for Strongly Light-Absorbing Carbonaceous Particles, *Aerosol Sci. Tech.*, 48, 777-788,  
403 10.1080/02786826.2014.919374, 2014.
- 404 Chen, H., Laskin, A., Baltrusaitis, J., Gorski, C. A., Scherer, M. M., and Grassian, V. H.: Coal Fly Ash  
405 as a Source of Iron in Atmospheric Dust, *Environ. Sci. Technol.*, 46, 2112-2120, 10.1021/es204102f,  
406 2012.
- 407 Cherian, R., Quaas, J., Salzmann, M., and Tomassini, L.: Black carbon indirect radiative effects in a  
408 climate model, *Tellus Ser. B-Chem. Phys. Meteorol.*, 69, 10.1080/16000889.2017.1369342, 2017.
- 409 Draxler, R. R., and Rolph, G. D.: HYSPLIT (HYbrid Single-Particle Lagrangian Integrated Trajectory)  
410 Model access via NOAA ARL READY Website, <http://ready.arl.noaa.gov/HYSPLIT.php>, NOAA Air  
411 Resources Laboratory, Silver Spring, MD, 2003.
- 412 Drewnick, F., Schneider, J., Hings, S. S., Hock, N., Noone, K., Targino, A., Weimer, S., and Borrmann,  
413 S.: Measurement of ambient, interstitial, and residual aerosol particles on a mountaintop site in central  
414 Sweden using an aerosol mass spectrometer and a CVI, *J. Atmos. Chem.*, 56, 1-20,  
415 10.1007/s10874-006-9036-8, 2007.
- 416 Dusek, U., Frank, G., Hildebrandt, L., Curtius, J., Schneider, J., Walter, S., Chand, D., Drewnick, F.,  
417 Hings, S., and Jung, D.: Size matters more than chemistry for cloud-nucleating ability of aerosol  
418 particles, *Science*, 312, 1375-1378, 10.1126/science.1125261, 2006.
- 419 Ebert, M., Weigel, R., Kandler, K., Günther, G., Molleker, S., Groß, J. U., Vogel, B., Weinbruch, S.,  
420 and Borrmann, S.: Chemical analysis of refractory stratospheric aerosol particles collected within the  
421 arctic vortex and inside polar stratospheric clouds, *Atmos. Chem. Phys.*, 16, 8405-8421,

422 10.5194/acp-16-8405-2016, 2016.

423 Eck, T. F., Holben, B. N., Reid, J. S., Xian, P., Giles, D. M., Sinyuk, A., Smirnov, A., Schafer, J. S.,  
424 Slutsker, I., Kim, J., Koo, J. H., Choi, M., Kim, K. C., Sano, I., Arola, A., Sayer, A. M., Levy, R. C.,  
425 Munchak, L. A., O'Neill, N. T., Lyapustin, A., Hsu, N. C., Randles, C. A., Da Silva, A. M., Buchard, V.,  
426 Govindaraju, R. C., Hyer, E., Crawford, J. H., Wang, P., and Xia, X.: Observations of the Interaction  
427 and Transport of Fine Mode Aerosols With Cloud and/or Fog in Northeast Asia from Aerosol Robotic  
428 Network (AERONET) and Satellite Remote Sensing, *J. Geophys. Res.-Atmos.*, 123, 5560-5587,  
429 10.1029/2018JD028313, 2018.

430 Ervens, B.: Modeling the Processing of Aerosol and Trace Gases in Clouds and Fogs, *Chem. Rev.*, 115,  
431 4157-4198, 10.1021/cr5005887, 2015.

432 Fan, J., Wang, Y., Rosenfeld, D., and Liu, X.: Review of Aerosol-Cloud Interactions: Mechanisms,  
433 Significance, and Challenges, *J. Atmos. Sci.*, 73, 4221-4252, 10.1175/jas-d-16-0037.1, 2016.

434 Farmer, D. K., Cappa, C. D., and Kreidenweis, S. M.: Atmospheric Processes and Their Controlling  
435 Influence on Cloud Condensation Nuclei Activity, *Chem. Rev.*, 115, 4199-4217, 10.1021/cr5006292,  
436 2015.

437 Fomba, K. W., van Pinxteren, D., Muller, K., Iinuma, Y., Lee, T., Collett, J. L., and Herrmann, H.: Trace  
438 metal characterization of aerosol particles and cloud water during HCCT 2010, *Atmos. Chem. Phys.*, 15,  
439 8751-8765, 10.5194/acp-15-8751-2015, 2015.

440 Hao, L., Romakkaniemi, S., Kortelainen, A., Jaatinen, A., Portin, H., Miettinen, P., Komppula, M.,  
441 Leskinen, A., Virtanen, A., Smith, J. N., Sueper, D., Worsnop, D. R., Lehtinen, K. E. J., and Laaksonen,  
442 A.: Aerosol Chemical Composition in Cloud Events by High Resolution Time-of-Flight Aerosol Mass  
443 Spectrometry, *Environ. Sci. Technol.*, 47, 2645-2653, 10.1021/es302889w, 2013.

444 Harris, E., Sinha, B., van Pinxteren, D., Tilgner, A., Fomba, K. W., Schneider, J., Roth, A., Gnauk, T.,  
445 Fahlbusch, B., and Mertes, S.: Enhanced role of transition metal ion catalysis during in-cloud oxidation  
446 of SO<sub>2</sub>, *Science*, 340, 727-730, 10.1126/science.1230911, 2013.

447 Hiranuma, N., Brooks, S. D., Moffet, R. C., Glen, A., Laskin, A., Gilles, M. K., Liu, P., Macdonald, A.  
448 M., Strapp, J. W., and McFarquhar, G. M.: Chemical characterization of individual particles and  
449 residuals of cloud droplets and ice crystals collected on board research aircraft in the ISDAC 2008 study,  
450 *J. Geophys. Res.-Atmos.*, 118, 6564-6579, 10.1002/jgrd.50484, 2013.

451 Hopkins, R. J., Desyaterik, Y., Tivanski, A. V., Zaveri, R. A., Berkowitz, C. M., Tylliszczak, T., Gilles, M.

452 K., and Laskin, A.: Chemical speciation of sulfur in marine cloud droplets and particles: Analysis of  
453 individual particles from the marine boundary layer over the California current, *J. Geophys.*  
454 *Res.-Atmos.*, 113, D04209, 10.1029/2007jd008954, 2008.

455 Hudson, J. G.: Variability of the relationship between particle size and cloud-nucleating ability,  
456 *Geophys. Res. Lett.*, 34, L08801, 10.1029/2006gl028850, 2007.

457 Ito, A., and Shi, Z.: Delivery of anthropogenic bioavailable iron from mineral dust and combustion  
458 aerosols to the ocean, *Atmos. Chem. Phys.*, 16, 85-99, 10.5194/acp-16-85-2016, 2016.

459 Kojima, T., Buseck, P. R., Wilson, J. C., Reeves, J. M., and Mahoney, M. J.: Aerosol particles from  
460 tropical convective systems: Cloud tops and cirrus anvils, *J. Geophys. Res.-Atmos.*, 109, D12201,  
461 10.1029/2003JD004504, 2004.

462 Li, J., Wang, X., Chen, J., Zhu, C., Li, W., Li, C., Liu, L., Xu, C., Wen, L., Xue, L., Wang, W., Ding, A.,  
463 and Herrmann, H.: Chemical composition and droplet size distribution of cloud at the summit of Mount  
464 Tai, China, *Atmos. Chem. Phys.*, 17, 9885-9896, 10.5194/acp-17-9885-2017, 2017a.

465 Li, W., Li, P., Sun, G., Zhou, S., Yuan, Q., and Wang, W.: Cloud residues and interstitial aerosols from  
466 non-precipitating clouds over an industrial and urban area in northern China, *Atmos. Environ.*, 45,  
467 2488-2495, 10.1016/j.atmosenv.2011.02.044, 2011a.

468 Li, W., Zhang, D., Shao, L., Zhou, S., and Wang, W.: Individual particle analysis of aerosols collected  
469 under haze and non-haze conditions at a high-elevation mountain site in the North China plain, *Atmos.*  
470 *Chem. Phys.*, 11, 11733-11744, 10.5194/acp-11-11733-2011, 2011b.

471 Li, W., Wang, Y., Collett, J. L., Chen, J., Zhang, X., Wang, Z., and Wang, W.: Microscopic Evaluation of  
472 Trace Metals in Cloud Droplets in an Acid Precipitation Region, *Environ. Sci. Technol.*, 47, 4172-4180,  
473 10.1021/es304779t, 2013.

474 Li, W., Shao, L., Zhang, D., Ro, C.-U., Hu, M., Bi, X., Geng, H., Matsuki, A., Niu, H., and Chen, J.: A  
475 review of single aerosol particle studies in the atmosphere of East Asia: morphology, mixing state,  
476 source, and heterogeneous reactions, *J. Clean Prod.*, 112, 1330-1349, 10.1016/j.jclepro.2015.04.050,  
477 2016a.

478 Li, W., Sun, J., Xu, L., Shi, Z., Riemer, N., Sun, Y., Fu, P., Zhang, J., Lin, Y., and Wang, X.: A  
479 conceptual framework for mixing structures in individual aerosol particles, *J. Geophys. Res.-Atmos.*,  
480 121, 13784-13798, 10.1002/2016JD025252, 2016b.

481 Li, W., Xu, L., Liu, X., Zhang, J., Lin, Y., Yao, X., Gao, H., Zhang, D., Chen, J., and Wang, W.: Air

482 pollution–aerosol interactions produce more bioavailable iron for ocean ecosystems, *Sci. Adv.*, 3,  
483 e1601749, 10.1126/sciadv.1601749, 2017b.

484 Lin, Q., Zhang, G., Peng, L., Bi, X., Wang, X., Brechtel, F. J., Li, M., Chen, D., Peng, P., Sheng, G., and  
485 Zhou, Z.: In situ chemical composition measurement of individual cloud residue particles at a mountain  
486 site, southern China, *Atmos. Chem. Phys.*, 17, 8473-8488, 10.5194/acp-17-8473-2017, 2017.

487 Liu, L., Kong, S., Zhang, Y., Wang, Y., Xu, L., Yan, Q., Lingaswamy, A. P., Shi, Z., Lv, S., Niu, H., Shao,  
488 L., Hu, M., Zhang, D., Chen, J., Zhang, X., and Li, W.: Morphology, composition, and mixing state of  
489 primary particles from combustion sources — crop residue, wood, and solid waste, *Sci. Rep.*, 7, 5047,  
490 10.1038/s41598-017-05357-2, 2017.

491 Liu, X., Wai, K. M., Wang, Y., Zhou, J., Li, P., Guo, J., Xu, P., and Wang, W.: Evaluation of trace  
492 elements contamination in cloud/fog water at an elevated mountain site in Northern China,  
493 *Chemosphere*, 88, 531-541, 10.1016/j.chemosphere.2012.02.015, 2012.

494 McFiggans, G., Artaxo, P., Baltensperger, U., Coe, H., Facchini, M. C., Feingold, G., Fuzzi, S., Gysel,  
495 M., Laaksonen, A., Lohmann, U., Mentel, T. F., Murphy, D. M., O'Dowd, C. D., Snider, J. R., and  
496 Weingartner, E.: The effect of physical and chemical aerosol properties on warm cloud droplet  
497 activation, *Atmos. Chem. Phys.*, 6, 2593-2649, 10.5194/acp-6-2593-2006, 2006.

498 Moffet, R. C., Desyaterik, Y., Hopkins, R. J., Tivanski, A. V., Gilles, M. K., Wang, Y., Shutthanandan, V.,  
499 Molina, L. T., Abraham, R. G., Johnson, K. S., Mugica, V., Molina, M. J., Laskin, A., and Prather, K. A.:  
500 Characterization of Aerosols Containing Zn, Pb, and Cl from an Industrial Region of Mexico City,  
501 *Environ. Sci. Technol.*, 42, 7091-7097, 10.1021/es7030483, 2008.

502 Pierce, J., Croft, B., Kodros, J., D'Andrea, S., and Martin, R.: The importance of interstitial particle  
503 scavenging by cloud droplets in shaping the remote aerosol size distribution and global aerosol-climate  
504 effects, *Atmos. Chem. Phys.*, 15, 6147-6158, 10.5194/acp-15-6147-2015, 2015.

505 Pratt, K. A., Twohy, C. H., Murphy, S. M., Moffet, R. C., Heymsfield, A. J., Gaston, C. J., DeMott, P. J.,  
506 Field, P. R., Henn, T. R., Rogers, D. C., Gilles, M. K., Seinfeld, J. H., and Prather, K. A.: Observation of  
507 playa salts as nuclei in orographic wave clouds, *J. Geophys. Res.-Atmos.*, 115, D15301,  
508 10.1029/2009jd013606, 2010.

509 Qi, J., Zheng, B., Li, M., Yu, F., Chen, C., Liu, F., Zhou, X., Yuan, J., Zhang, Q., and He, K.: A  
510 high-resolution air pollutants emission inventory in 2013 for the Beijing-Tianjin-Hebei region, China,  
511 *Atmos. Environ.*, 170, 156-168, 10.1016/j.atmosenv.2017.09.039, 2017.



512 Qian, Y., Gong, D., Fan, J., Leung, L. R., Bennartz, R., Chen, D., and Wang, W.: Heavy pollution  
513 suppresses light rain in China: Observations and modeling, *J. Geophys. Res.-Atmos.*, 114, D00K02,  
514 10.1029/2008JD011575, 2009.

515 Roberts, J. R., Taylor, M. D., Castranova, V., Clarke, R. W., and Antonini, J. M.: Soluble metals  
516 associated with residual oil fly ash increase morbidity and lung injury after bacterial infection in rats, *J.*  
517 *Toxicol. Env. Health Part A*, 67, 251-263, 10.1080/15287390490266927, 2004.

518 Rosenfeld, D.: Suppression of rain and snow by urban and industrial air pollution, *Science*, 287,  
519 1793-1796, 10.1126/science.287.5459.1793, 2000.

520 Rosenfeld, D., Sherwood, S., Wood, R., and Donner, L.: Climate effects of aerosol-cloud interactions,  
521 *Science*, 343, 379-380, 10.1126/science.1247490, 2014.

522 Roth, A., Schneider, J., Klimach, T., Mertes, S., van Pinxteren, D., Herrmann, H., and Borrmann, S.:  
523 Aerosol properties, source identification, and cloud processing in orographic clouds measured by single  
524 particle mass spectrometry on a central European mountain site during HCCT-2010, *Atmos. Chem.*  
525 *Phys.*, 16, 505-524, 10.5194/acp-16-505-2016, 2016.

526 Schneider, J., Mertes, S., Pinxteren, D. v., Herrmann, H., and Borrmann, S.: Uptake of nitric acid,  
527 ammonia, and organics in orographic clouds: mass spectrometric analyses of droplet residual and  
528 interstitial aerosol particles, *Atmos. Chem. Phys.*, 17, 1571-1593, 10.5194/acp-17-1571-2017, 2017.

529 Schroder, J., Hanna, S., Modini, R., Corrigan, A., Kreidenweis, S., Macdonald, A., Noone, K. J., Russell,  
530 L., Leitch, W., and Bertram, A.: Size-resolved observations of refractory black carbon particles in  
531 cloud droplets at a marine boundary layer site, *Atmos. Chem. Phys.*, 15, 1367-1383,  
532 10.5194/acp-15-1367-2015, 2015.

533 Seinfeld, J. H., and Pandis, S. N.: *Atmospheric chemistry and physics: from air pollution to climate*  
534 *change*, John Wiley & Sons, 2006.

535 Seinfeld, J. H., Bretherton, C., Carslaw, K. S., Coe, H., DeMott, P. J., Dunlea, E. J., Feingold, G., Ghan,  
536 S., Guenther, A. B., Kahn, R., Kraucunas, I., Kreidenweis, S. M., Molina, M. J., Nenes, A., Penner, J. E.,  
537 Prather, K. A., Ramanathan, V., Ramaswamy, V., Rasch, P. J., Ravishankara, A. R., Rosenfeld, D.,  
538 Stephens, G., and Wood, R.: Improving our fundamental understanding of the role of aerosol-cloud  
539 interactions in the climate system, *Proc. Natl. Acad. Sci. U.S.A.*, 113, 5781-5790,  
540 10.1073/pnas.1514043113, 2016.

541 Shen, X. H., Lee, T., Guo, J., Wang, X., Li, P., Xu, P., Wang, Y., Ren, Y., Wang, W., Wang, T., Li, Y.,

542 Cam, S. A., and Collett, J. L.: Aqueous phase sulfate production in clouds in eastern China, *Atmos.*  
543 *Environ.*, 62, 502-511, 10.1016/j.atmosenv.2012.07.079, 2012.

544 Tilgner, A., Schöne, L., Bräuer, P., Van Pinxteren, D., Hoffmann, E., Spindler, G., Styler, S., Mertes, S.,  
545 Birmili, W., and Otto, R.: Comprehensive assessment of meteorological conditions and airflow  
546 connectivity during HCCT-2010, *Atmos. Chem. Phys.*, 14, 9105-9128, 10.5194/acp-14-9105-2014,  
547 2014.

548 Twohy, C. H., and Anderson, J. R.: Droplet nuclei in non-precipitating clouds: composition and size  
549 matter, *Environ. Res. Lett.*, 3, 10.1088/1748-9326/3/4/045002, 2008.

550 Ueda, S., Hirose, Y., Miura, K., and Okochi, H.: Individual aerosol particles in and below clouds along a  
551 Mt. Fuji slope: Modification of sea-salt-containing particles by in-cloud processing, *Atmos. Res.*, 137,  
552 216-227, 10.1016/j.atmosres.2013.10.011, 2014.

553 Wang, J., Cubison, M. J., Aiken, A. C., Jimenez, J. L., and Collins, D. R.: The importance of aerosol  
554 mixing state and size-resolved composition on CCN concentration and the variation of the importance  
555 with atmospheric aging of aerosols, *Atmos. Chem. Phys.*, 10, 7267-7283, 10.5194/acp-10-7267-2010,  
556 2010.

557 Wang, Y., Guo, J., Wang, T., Ding, A., Gao, J., Zhou, Y., Collett, J. L., and Wang, W.: Influence of  
558 regional pollution and sandstorms on the chemical composition of cloud/fog at the summit of Mt.  
559 Taishan in northern China, *Atmos. Res.*, 99, 434-442, 10.1016/j.atmosres.2010.11.010, 2011.

560 Wang, Z., Zhang, H., Li, J., Jing, X., and Lu, P.: Radiative forcing and climate response due to the  
561 presence of black carbon in cloud droplets, *J. Geophys. Res.-Atmos.*, 118, 3662-3675,  
562 10.1002/jgrd.50312, 2013.

563 Zhang, D., Ishizaka, Y., and Aryal, D.: Individual particles and droplets in continentally influenced  
564 stratocumulus: A case study over the Sea of Japan, *Atmos. Res.*, 79, 30-51,  
565 10.1016/j.atmosres.2005.04.003, 2006.

566 Zhang, G., Lin, Q., Peng, L., Bi, X., Chen, D., Li, M., Li, L., Brechtel, F. J., Chen, J., Yan, W., Wang, X.,  
567 Peng, P., amp, apos, an, Sheng, G., and Zhou, Z.: The single-particle mixing state and cloud scavenging  
568 of black carbon: a case study at a high-altitude mountain site in southern China, *Atmos. Chem. Phys.*,  
569 17, 14975-14985, 10.5194/acp-17-14975-2017, 2017.

570 Zhang, Y. M., Zhang, X. Y., Sun, J. Y., Hu, G. Y., Shen, X. J., Wang, Y. Q., Wang, T. T., Wang, D. Z.,  
571 and Zhao, Y.: Chemical composition and mass size distribution of PM<sub>1</sub> at an elevated site in central east

572 China, *Atmos. Chem. Phys.*, 14, 12237-12249, 10.5194/acp-14-12237-2014, 2014.

573 Zhao, C., Tie, X., and Lin, Y.: A possible positive feedback of reduction of precipitation and increase in  
574 aerosols over eastern central China, *Geophys. Res. Lett.*, 33, L11814, 10.1029/2006gl025959, 2006.

575 Zuberi, B., Johnson, K. S., Aleks, G. K., Molina, L. T., and Laskin, A.: Hydrophilic properties of aged  
576 soot, *Geophys. Res. Lett.*, 32, L01807, 10.1029/2004gl021496, 2005.

577